Series-Fed Antenna Array without Beam Deterioration Using Miniaturized Bandpass Filters for Phase-Slope Balancing

Huanhuan Shi[1], Xin Guo[1, 2, *], and Wen Wu[1]

Abstract—A design of a series-fed antenna array without beam deterioration using miniaturized bandpass filters (BPFs) is proposed. The BPFs are connected behind branches of series feed network (SFN) to compensate the varied phase slope of paths, resulting in constant phase difference between elements across the bandwidth. Hence, the beam deterioration versus frequency is removed. The closed-form equations of the phase slopes for BPFs are deduced, and thus they can be designed quantitatively for phase slope balancing. The proposed SFN has advantages of compactness, simplicity, and low loss. For validation, an 8-element antenna array is designed and measured. The gain and sidelobe level are 12.2–12.39 dBi and 11.67–12.65 dB within the bandwidth of 5.2–5.8 GHz. As comparison, the gain and sidelobe level are 12.85–13.77 dBi and 7.18–12.75 dB using conventional feed network. Therefore, the designed antenna array has stable radiation pattern including beam direction, sidelobe level, and gain.

1. INTRODUCTION

Feed network for antenna array is a major design concern in terms of complexity and performance. Conventional methods to achieve required excitation include series and parallel feed networks [1]. Comparatively, the series feed network (SFN) is simpler, more compact, and less lossy. However, it suffers from an inherent problem of beam deterioration. This limits the applications of series-fed antenna in point-to-point communication system which usually needs an antenna with a stable radiation pattern in its operating band.

To solve the beam deterioration problem, various methods have been put forward. In [2], a circuit with phase advance and negative group delay (NGD) is proposed and used in the series-fed array to reduce the variation of beam angle and gain. In [3], transmission lines (TLs) between junction points are loaded with NGD networks for squint-free radiation. In [4], a dispersion-engineered artificial TL enabled by NGD network is proposed to exhibit squint-free leaky-wave radiation. Recently, the reconfigurable NGD circuits proposed in [5] and [6] are applied to create tunable squint-free beamforming networks. The NGD circuits could effectively reduce the beam deterioration, but they suffer from high loss, and the power amplifiers are usually used for loss compensation.

The degree of freedom provided by the length and propagation constant of TLs is used to eliminate beam deterioration. In [7, 9], it is proposed that by the employment of either varying length TLs or the same length TLs with varying phase constant in branches, the beam deterioration can be eliminated. The above works are implemented by controlling the characteristic of conventional TLs involving length and phase constant. However, these designs usually need relatively long TLs to connect the antenna, which is necessary for dispersion engineering.

Some kinds of artificial transmission lines are also used. In [10], the dispersion engineered lines to reduce beam-deterioration radiation is investigated. Left-handed (LH) lines are used to compensate the

---

[1] Key Laboratory of Near-Range RF Sensing ICs & Microsystems (NJUST), Ministry of Education, Nanjing University of Science and Technology, Nanjing 210094, China. [2] State Key Laboratory of Millimeter Waves, Southeast University, Nanjing 210096, China.

group delay of branches, so that the group delay to each output port is almost equal. The series-fed networks using composite right/left handed transmission line (CRLH-TL) to reduce beam-deterioration radiation are published in [11–14]. However, these complex designs occupy a large size. Negative-refractive-index transmission line (NRI-TL) metamaterial is used to reduce beam deterioration in series-fed antennas [15] and leaky-wave antennas [16, 17]. However, these methods can usually reduce, rather than eliminate, the beam deterioration.

In our early work [18], a tunable phase shifter with phase slope tunability is designed with the use of filter theory. On this basis, in this article, a series-fed antenna array without beam deterioration using miniaturized bandpass filters (BPFs) is proposed. Miniaturized BPFs are used to balance the phase slopes in paths of the SFN, resulting in a series-fed array with stable phase difference between signal paths. It has advantages of compact size, easy design, and low loss. An 8-element series-fed patch array is designed and fabricated for validation. The radiation performances including beam direction, side lobe level, and gain across the bandwidth are more stable than its conventional series-fed counterpart.

2. BASIC THEORY AND DESIGN METHOD

2.1. Conventional Series Feed Network

Figure 1 depicts the scheme of a conventional four-element series-fed network which is under equal distribution. The interelement spacing between output ports is set as one guide wavelength ($\theta = 360°$), in order to make the power arrive in-phase at each output port. Herein, the input and output port impedances are set as $Z = 50\,\Omega$ and $Z_L = 75\,\Omega$, respectively. Now, let's concentrate on the design of line impedances (Z_1, Z_2, and Z_3). In this network, the line impedances are deliberately set as:

$$Z_i = \frac{1}{i}Z_L \tag{1}$$

where $i = 1$, 2, and 3. In this way, at each power dividing junction, the following relations are kept:

$$Z_{in,i} = \frac{1}{1+n}Z_L = Z_{i+1}, \quad \frac{P_{ti}}{P_L} = \frac{Z_L}{Z_{in,i-1}} = \frac{n}{1} \tag{2}$$

where $Z_{in,\,i}$ is the input impedance of the ith junction, P_{ti} the power transferred to the next junction, and P_L the power transferred to the load termination. To match the input impedance of the 3rd junction to Z, a $\lambda_g/4$ transformer is used, and the characteristic impedance is

$$Z_T = \sqrt{Z_0 \frac{Z_L}{4}} \tag{3}$$

Thus, all the parameters in Fig. 1 are calculated as: $Z_1 = 75\,\Omega$, $Z_2 = 37.5\,\Omega$, $Z_3 = 25\,\Omega$, $Z_T = 30.62\,\Omega$, $\theta = 360°$, and $\theta_T = 90°$.
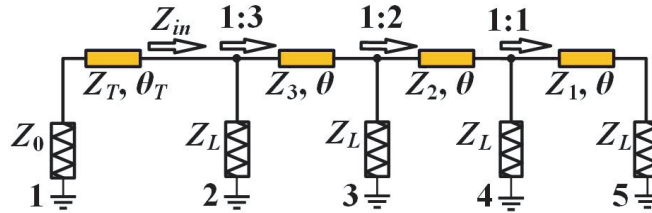
Figure 1. Scheme of a conventional four-element series-fed network.

The magnitude and phase responses versus normalized frequency of the feed network are simulated and plotted in Fig. 2. As can be seen, Fig. 2(a) shows a good input matching, and the power from the input to each output port is close to ideal $-6\,$dB over a wide bandwidth. In Fig. 2(b), the phase difference among paths is exactly $360°$ at the central frequency (f). However, when the frequency is deviated from f, the phase difference is also changed. It is because the electrical length of the signal path increases from input port 1 to output ports 2–5, thus the phase slope grows accordingly, which can also be observed in Fig. 2(b). As a result, the phase difference is changed with respect to frequency, which will lead to beam deterioration.
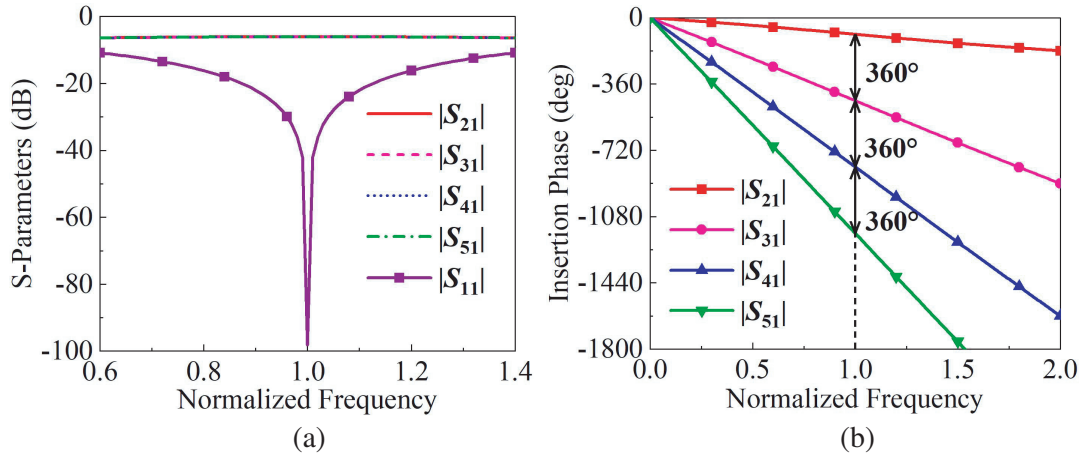
Figure 2. Simulated magnitude and phase responses of conventional series-fed network in Fig. 1. (a) Magnitude. (b) Transmission phase.

2.2. Bandpass Filters for Phase Slope Balancing

Based on Section 2.1, as shown in Fig. 3(a), the miniaturized filter with different phase slopes is connected behind each branch to construct a series network with constant phase difference across the bandwidth. Figs. 3(b) and (c) display the work mechanism of the proposed network, from the perspective of phase response. For conventional SFN, the lengths of signal paths are increased from input port 1
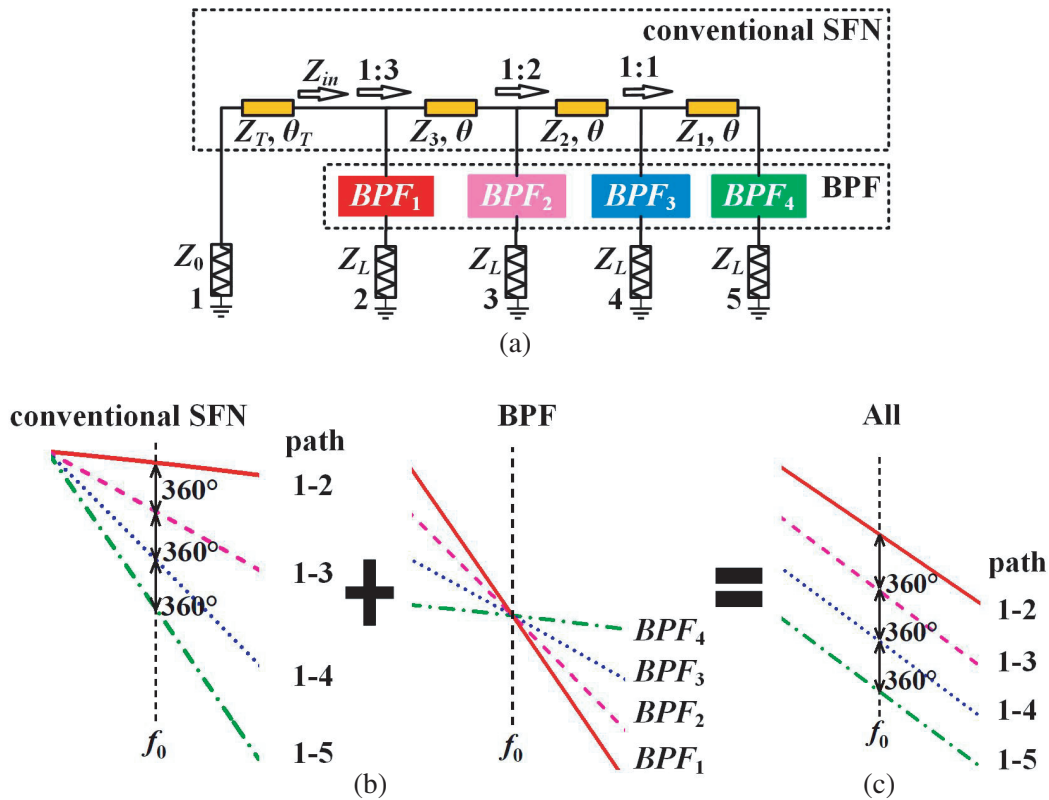
Figure 3. (a) Scheme of the proposed series-fed network without beam deterioration. (b) Phase responses of series power divider and BPFs. (c) Phase responses of the whole feeding network.

to ports 2 to 5, thus their phase slopes become larger accordingly. Meanwhile, for the BPFs, they have the same transmission phases at f. More importantly, the phase slopes of BPFs connected to ports 2 to 5 show a decreasing trend. By connecting the BPFs with decreasing phase slopes to the SFN with increasing phase slopes, the overall structure will obtain the constant phase slopes in four paths. As shown in the last figure in Fig. 3, it is theoretically possible to realize the constant $360°$ phase difference, with no beam deterioration.

From the basic theory above, to construct an SFN without beam deterioration, the phase and phase slope of the BPF in each branch should be designed carefully. First, the phase difference of these BPFs at f should be either $0°$ or an integer multiple of $360°$. It is achieved by a proper selection of the filter order. Fig. 4(a) shows the transmission phase response of ideal Chebyshev BPF with different orders under the same bandwidth and return loss (RL). From Fig. 4(a), when the order of BPF increases by one, the transmission phase at f increases by $90°$. For simplicity and compactness, the 2nd and 4th-order BPFs are selected with the phase difference of $180°$ at f. Then, the other phase difference of $180°$ should be compensated. Here, the phase difference of $180°$ brought in by voltage distribution of $\lambda_g/2$ resonator is utilized. As conceptually shown in Fig. 4(b), the voltage on $\lambda_g/2$ resonator is out-of-phase at the two sides of the resonator. In this way, designing the filter with the feeding position at P and at the symmetric P' will generate a phase difference of $180°$.
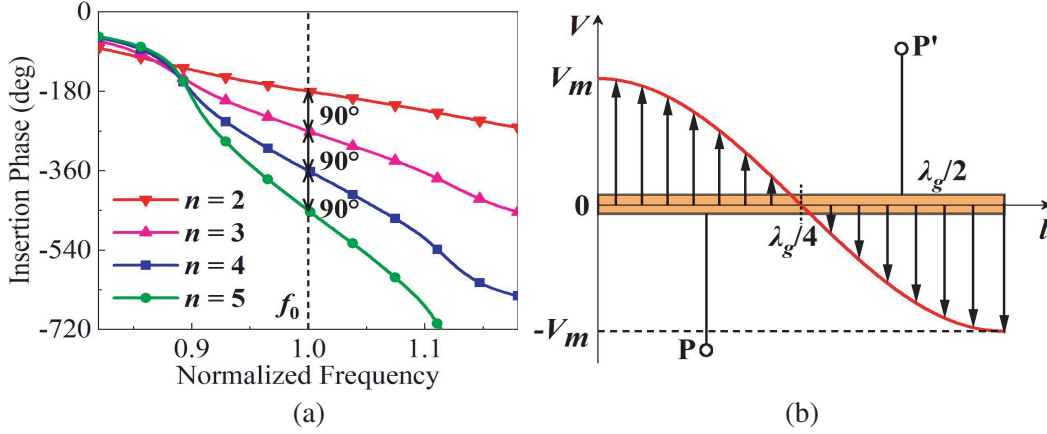
Figure 4. (a) Transmission phase response of ideal Chebyshev BPF with different order. (b) $180°$ phase difference brought in by voltage distribution of $\lambda_g/2$ resonator at different feeding positions.

Next, the physical structures of BPFs need to be determined. Fig. 5 displays the compact coupled resonator filters of 2nd- and 4th-order, respectively. For the 2nd-order filter, two $\lambda_g/2$ resonators are used and coupled together to construct the filter. For the 4th-order filter, four $\lambda_g/4$ resonators are used and coupled together through via-holes (equivalent K-inverter) and coupled lines (equivalent J-inverter) in sequence. It needs to be mentioned here that the $\lambda_g/2$ resonators are utilized in the 2nd-order filter because the out-of-phase voltage distribution could be utilized for $180°$ phase difference, and $\lambda_g/4$ resonators are utilized in the 4th-order filter for the purpose of a compact size. With the use of $\lambda_g/4$ resonators, the 4th-order filter has almost the same size as the 2nd-order filter.

Now, let us start with the analysis of the phase slope properties. The equivalent circuit models of 2nd- and 4th-order filters are plotted in Fig. 6. The S matrices of the two BPFs can be derived in terms of $ABCD$-matrix using the well-known network theorem. The $ABCD$-matrix of the 2nd-order BPF is expressed by (4).

$$\begin{bmatrix} A & B \\ C & D \end{bmatrix} = [J_1][R][J_2][R][J_1] \tag{4}$$

Here, $[J_i]$ is the $ABCD$-matrix for J_i inverter ($i = 1$ and 2), and $[R]$ is the matrix for resonator. The output phase $\angle S_{21}$ of the 2nd-order BPF can be explicitly derived in terms of the overall $ABCD$-matrix
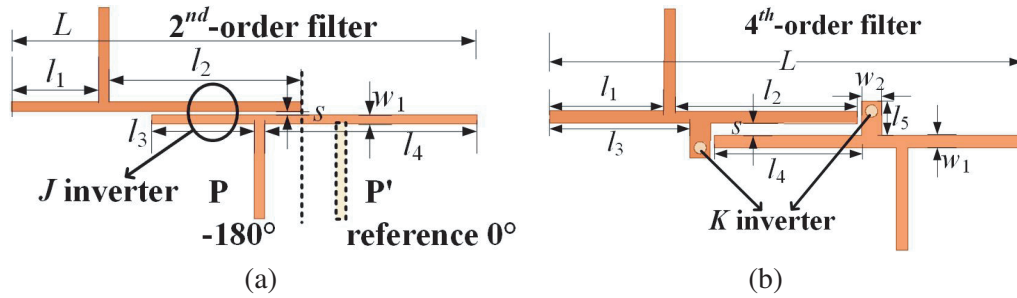
Figure 5. Physical structures of (a) 2nd-order and (b) 4th-order BPFs.

in (4).

$$\angle S_{21} = -\tan^{-1} \frac{B/Z_0 + CZ_0}{j(A+D)} \qquad (5)$$

Then, the phase slope of the 2nd-order BPF at f can be quantitatively deduced as

$$\left. \frac{d\angle S_{21}}{d\theta} \right|_{\theta=\pi} = \frac{f_0}{\pi} \left. \frac{d\angle S_{21}}{df} \right|_{f=f_0} = -\frac{4g_1 g_2}{FBW\pi(g_1+g_2)} - \frac{FBW\pi}{g_1+g_2} \qquad (6)$$

Similarly, we can derive the phase slope of the 4th-order BPF at f as

$$\left. \frac{d\angle S_{21}}{d\theta} \right|_{\theta=\pi/2} = \frac{2f_0}{\pi} \left. \frac{d\angle S_{21}}{df} \right|_{f=f_0} = -\frac{8g_2(g_1+g_3)}{FBW\pi(g_2+g_3)} - \frac{FBW\pi(g_1+g_3)}{2g_1(g_2+g_3)} \qquad (7)$$

g_0, g_1, ..., g_N are element values of the Nth-order Chebyshev lowpass prototype filter, and FBW is defined as fractional bandwidth. Using (6) and (7), Fig. 6 also plots the phase slope curves of 2nd- and 4th-order filters with respect to FBW. Herein, the Chebyshev lowpass prototype filter is with bandpass ripple $L_{Ar} = 0.1\,\mathrm{dB}$, then values of g_i are determined. Form Fig. 6, for both filters, the phase slopes first rise rapidly and then slowly, with the change of FBW. Specifically, the 4th-order filter has a larger phase slope value than that of the 2nd-order filter, under the same FBW and RL. Based on (6) and (7), the BPF in each branch can be designed quantitatively. In our design, the phase difference between two adjacent paths in SFN is $\Delta\Phi = 360°$. So we should carefully design the phase slope values of BPFs to balance the phase slope of 360° lines.
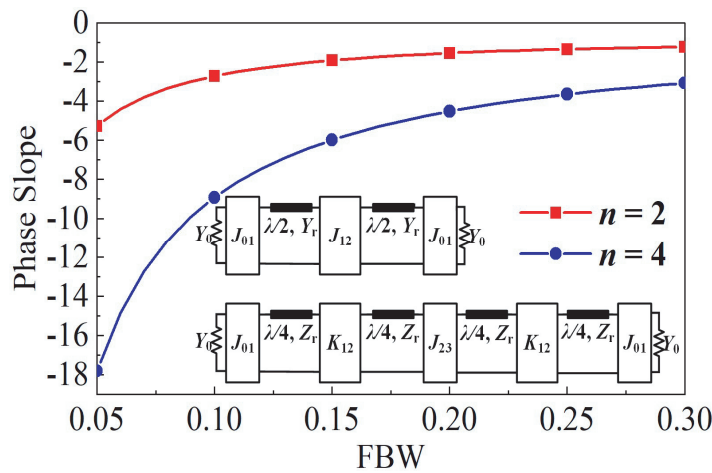
Figure 6. Phase slope curves of 2nd-order and 4th-order BPFs.

2.3. Design Example

After the theory of the proposed SFN without beam deterioration is clearly demonstrated as above, a detailed design example is exhibited. At the beginning of Section 2, the conventional SFN is designed. Here, the BPF connected behind each branch should be carefully determined. As shown in Fig. 7(a), the BPF is connected behind each branch, and the electrical length of lines between each two adjacent branches is 360°. To achieve constant phase difference across the bandwidth, the phase slope of each two adjacent paths should be identical at f, that is

$$\left.\frac{d\angle BPF_i(f)}{df}\right|_{f=f_0} + \frac{\Delta\Phi}{f_0} = \left.\frac{d\angle BPF_{i+1}(f)}{df}\right|_{f=f_0} \tag{8}$$

where $i = 1$, 2, and 3. We choose one reference branch as 0° and assign $L_{Ar} = 0.1\,\text{dB}$ and FBW = 10% to its 2nd-order filter. Then, the FBW of other filters can be calculated, with $L_{Ar} = 0.1\,\text{dB}$ as well. Considering the interaction among branches in SFN, the calculated values are slightly optimized, and the final specifications are determined, as shown in Fig. 7(a). BPF_1 and BPF_2 use 4th-order BPFs with FBWs of 18% and 21.6%, and BPF_3 and BPF_4 use 2nd-order BPFs with FBWs of 10% and 13.5%, respectively. Fig. 7(b) plots the simulated magnitude and phase response versus normalized frequency of these FBWs. The phases of the filters are equal at f. And the phase slope values of BPF_n ($n = 1, \ldots, 4$) have a decreasing trend between each two adjacent branches. Additionally, the difference between adjacent phase slopes is almost same with the phase slope value of 360° line.
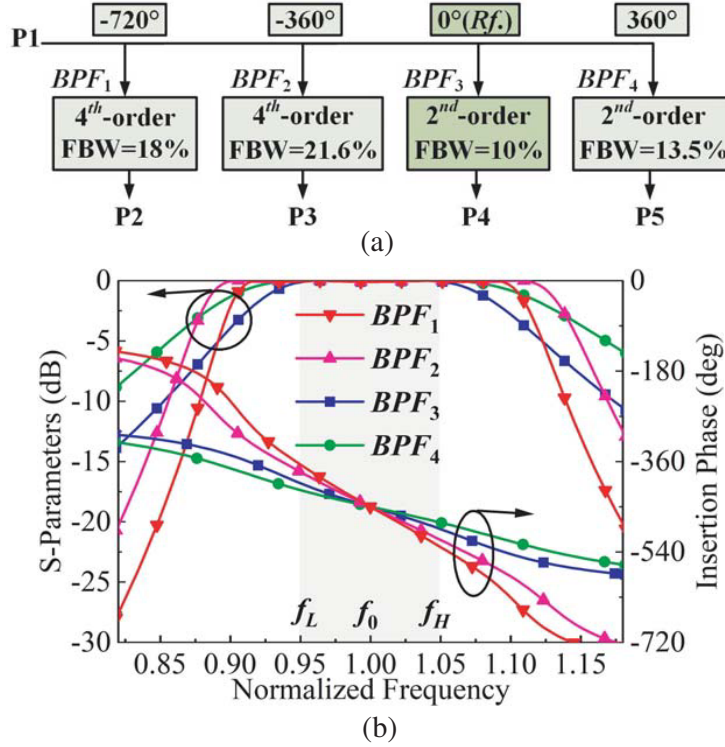
Figure 7. (a) Quantitatively specification of BPFs in proposed series-fed network without beam deterioration. (b) Simulated magnitude and phase response of BPF_n ($n = 1, \ldots, 4$) versus normalized frequency.

3. SIMULATION AND EXPERIMENT

To experimentally validate the proposed SFN without beam deterioration, an 8-way series-fed antenna array with f of 5.5 GHz is designed, fabricated, and measured. This SFN is built on a Rogers RO4003C

($\varepsilon_r = 3.55$, $\tan \delta = 0.0027$) substrate with the thickness (h_1) of 0.508 mm. Fig. 8(a) shows TL model of this 8-element series-fed array. Two 4-way SFNs are shunt connected to form 8-way SFN. θ_1 is selected as $360°$, comprehensively considering antenna locations and the physical layout of BPFs. Based on the matching theory, $Z_4 = Z_L/4 = 18.75\,\Omega$. Thus, the input impedance is $Z_L/8$. And it needs to match $Z = 50\,\Omega$, so $Z_T = 21.65\,\Omega$. Then, the physical dimensions can be mapped from these derived characteristic impedances and electrical lengths by using ADS Linecalc Tools. The specifications of 2nd- and 4th-order BPFs have been determined in Section 2.3, and they are implemented on physical structures just following basic filter design method. The detailed dimensions of all the filters used in the designed array are listed in Table 1. The antenna element used in this design follows the one in [19] which has a wide bandwidth, stable radiation pattern, and simple structure. The geometry and dimensions of the wideband microstrip patch antenna are given in Fig. 8(b). The patch antennas are built on an FR4 substrate with ε_r of 4.4 and thickness (h_2) of 4 mm. Fig. 8(c) shows three-dimensional view of the overall structure. The feed network and antennas are printed on two separate substrates and assembled back-to-back sharing the common middle ground. Metallic pins passing through the common ground plane are used to connect them.
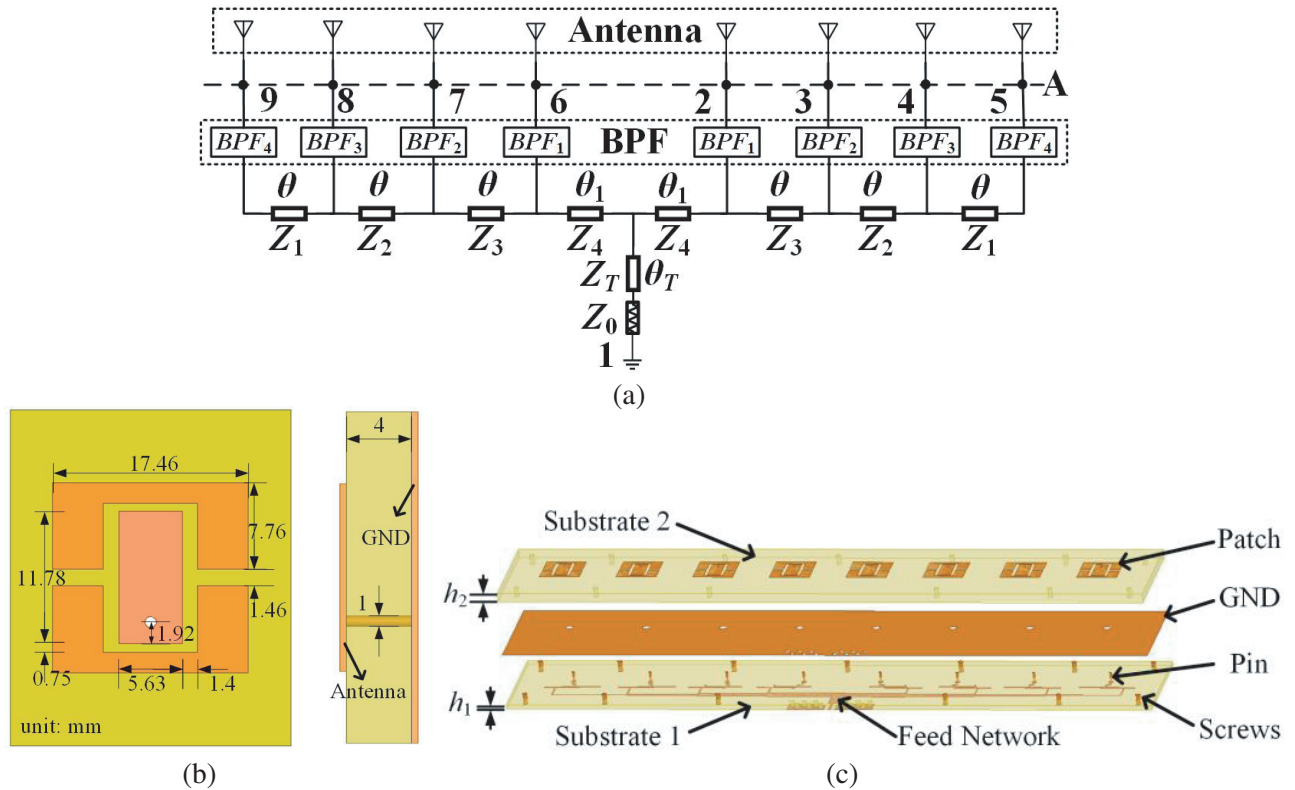
Figure 8. Designed 8-element series-fed array without beam deterioration. (a) Transmission line model. (b) Geometry and dimensions of the microstrip patch antenna. (c) Three-dimensional view.

Table 1. Detailed dimensions of all the filters used in the designed array.

filters	L (mm)	l_1 (mm)	l_2 (mm)	l_3 (mm)	l_4 (mm)	l_5 (mm)	s (mm)	w_1 (mm)	w_2 (mm)
BPF_1	23.682	5.868	8.978	7.086	7.31	1.513	0.717	1	0.6
BPF_2	23.294	5.648	8.968	6.928	7.238	1.701	0.598	1	0.6
BPF_3	25.246	5.054	10.051	5.623	10.618	-	0.258	-	0.6
BPF_4	24.713	4.634	10.191	5.451	11.27	-	0.169	-	0.5

The full-wave simulation is executed by ANSYS HFSS 15.0, and the measurement is carried out using vector network analyzer Agilent N5244A. The radiation performance is experimentally verified inside an anechoic chamber. Figs. 9(a) and (b) show simulated magnitude and phase responses of the designed feed network at the reference plane A. From the figures, it is obvious that the signals at output ports keep equal and in-phase across the bandwidth.
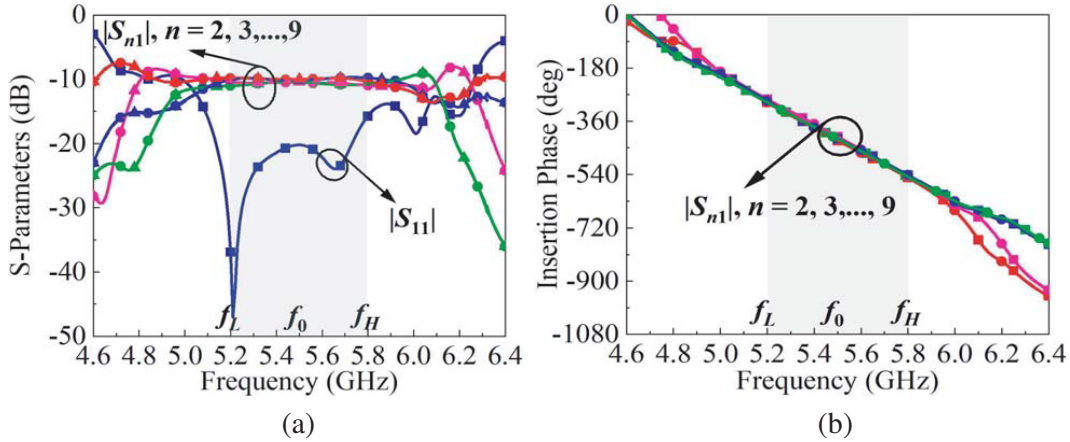
Figure 9. (a) Simulated magnitude of designed feed network. (b) Phase response of designed feed network.

Definitely different from the simulated results of conventional SFN in Fig. 2, the phase difference keeps unchanged with respect to the frequency. There will be no beam deterioration, when the frequency is deviated from f.

Figures 10(a) and (b) depict the simulated gain curves of the conventional array using SFN in Fig. 1 and the proposed array using the network in Fig. 7. In the two figures, it is obvious that the sidelobe in Fig. 10(a) is deteriorated dramatically, and the gain is changed, when the frequency is within points of interest. However, with the use of the proposed feed network, the antenna array has more stable sidelobe level (SLL) and gain across the bandwidth. Specifically, the gain and SLL are 12.85–13.77 dBi and 7.18–12.75 dB in Fig. 10(a), respectively. As comparison, the gain and SLL are 12.2–12.39 dBi and 11.67-12.65 dB in Fig. 10(b), respectively.

The series-fed array shown in Fig. 8(c) is fabricated and measured. As can be observed in Fig. 11, the simulated and measured results are found in good agreement with each other. A bit mismatch in
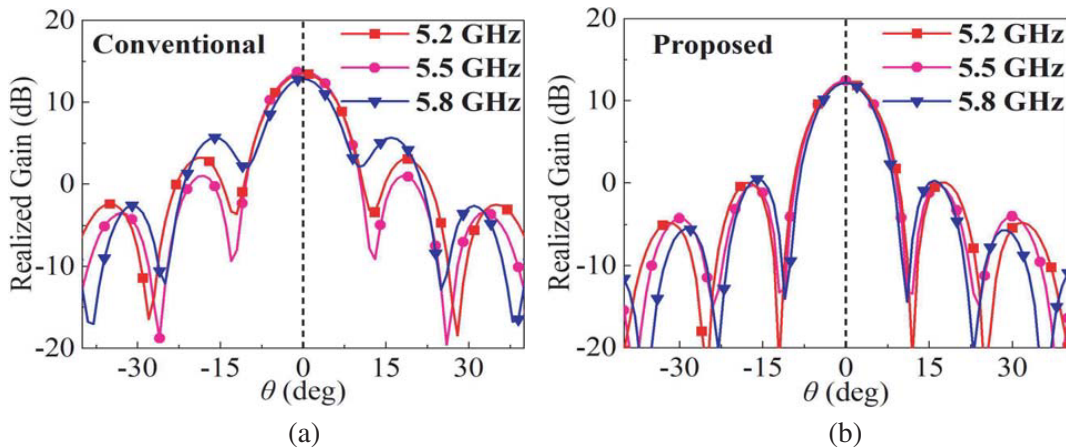
Figure 10. Simulated gains of the series-fed array. (a) Using conventional SFN in Fig. 1. (b) Using proposed network in Fig. 7.
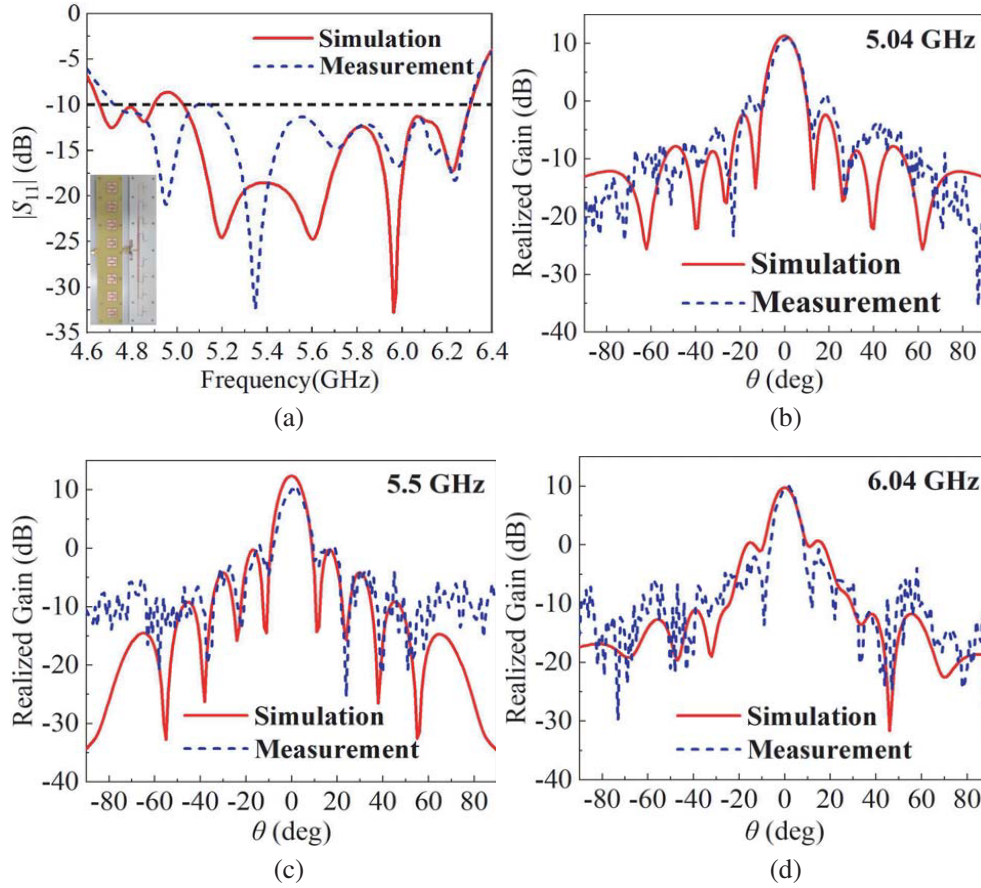
Figure 11. (a) Simulated and measured reflection coefficients for design antenna array. And realized gain patterns of design antenna array at (b) 5.04, (c) 5.5, and (d) 6.04 GHz.

Fig. 11(a) may be caused by the potential poor contact between the FR4 substrate and the RO4003C substrate. The measured impedance bandwidth of the antenna array is 28.73% (from 4.72 to 6.3 GHz) with $|S_{11}| < 9.96$ dB. From 5.04 to 6.04 GHz, the radiation pattern is stable with sidelobe level of 9–12.2 dB and gain of 9.6–11.9 dBi. The radiation patterns at 5.04, 5.5, and 6.04 GHz are plotted in Figs. 11(b)–(d).

Table 2. Comparison with other similar works.

Refs.	Method	Number of Elements	Beam Deviation	SLL (dB)	Insertion Loss (dB)	Additional Space
[3]	NGD	4	$-1.9°$–$0.1°$	$> -7^*$	6^*	Yes
[8]	TL	16	$-2°$–$2°$	$> -6^*$	-	Yes
[9]	TL	4	$-2°$–$2°$	-	1.5^* / 2^*	Yes
[12]	CRLH-TL	3	$-7.38°$–$3.21°$ / $-1.36°$–$0.89°$	-	0.56 / 1.48	Yes
[15]	NRI-TL	4	$-2°$–$4°$	$> -6^*$	-	No
This work	Filter network	8	$0°$	> -11.67	1.516	No

* denotes the data is read from figures.

The comparison with other similar works is tabulated in Table 2. In terms of performance, the proposed network solves the problem of beam deviation (for side fed) or sidelobe deterioration (for central fed) with frequency, and has the advantage of low loss. In terms of physical structure, the proposed feed network has the advantage of small size, which does not need additional space array as shown in Fig. 8(c).

With the further expansion of the array size, on the one hand, the large-scale array can be decomposed into subarrays, and the group delay regulator can be introduced among the sub-arrays; on the other hand, the filtering antenna element or subarray could be used for phase balancing, thus the additional filter is reduced resulting in simpler structure and lower loss. For both schemes, the proposed design theory is still valid.

4. CONCLUSION

A novel series-fed network using miniaturized filters is proposed to remove the beam deterioration. The closed-form equations of the phase slopes for BPFs are deduced, thus they can be designed according to required phase slopes quantitatively. By connecting BPFs for phase slope balancing, the equal power can arrive at output ports with constant phase difference across the bandwidth. An example of an 8-element array is designed for validation. The antenna has the stable gain of 12.2–12.39 dBi and sidelobe level of 11.67–12.65 dB within 5.2–5.8 GHz. In conclusion, compared with the conventional one, the proposed network owns the advantages of compactness, simplicity, and low loss. Besides, radiation patterns of the designed antenna array have stable SLL and gain within the bandwidth. In the future, the 8-element antenna array can be expanded to an antenna array with more elements, which will require more appropriate filtering structures and more novel design.

ACKNOWLEDGMENT

REFERENCES

1. Stutzman, W. L. and G. A. Thiele, *Antenna Theory and Design*, 2nd Edition, Wiley, New York, 1998.
2. Oh, S.-S. and L. Shafai, "Compensated circuit with characteristics of lossless double negative materials and its application to array antennas," *IET Microw. Antennas Propag.*, Vol. 1, No. 1, 29–38, Feb. 2007.
3. Mirzaei, H. and G. V. Eleftheriades, "Arbitrary-angle squint-free beamforming in series-fed antenna arrays using non-Foster elements synthesized by negative-group-delay networks," *IEEE Trans. Antennas Propag.*, Vol. 63, No. 5, 1997–2010, May 2015.
4. Zhu, M. and C.-T. M. Wu, "Negative group delay enabled artificial transmission line exhibiting squint-free, dominant mode, backward leakywave radiation," *IEEE MTT-S Int. Microw. Symp. Dig.*, 309–312, Los Angeles, CA, USA, Aug. 2020.
5. Zhu, M. and C.-T. M. Wu, "Reconfigurable series feed network for squint-free antenna beamforming using distributed amplifier-based negative group delay circuit," *Proc. 49th Eur. Microw. Conf. (EuMC)*, 256–259, Paris, France, Oct. 2019.
6. Zhu, M. and C.-T. M. Wu, "Reconfigurable non-Foster elements and squint-free beamforming networks using active transversal filter-based negative group delay circuit," *IEEE Trans. Microw. Theory Techn.*, Vol. 70, No. 1, 222–231, Jan. 2022.
7. Fonseca, N. J. G., A. Ali, and H. Aubert, "Cancellation of beam squint with frequency in serial beamforming network-fed linear array antennas," *IEEE Antennas Propag. Mag.*, Vol. 54, No. 1, 32–39, Feb. 2012.

8. Cai, S. and J. Liu, "A printed wideband squintless traveling-wave antenna," *IEEE Antennas Wireless Propag. Lett.*, Vol. 20, No. 8, 1473–1477, Aug. 2021.

9. Mirzaei, H. and G. V. Eleftheriades, "Eliminating beam-deterioration in wideband linear series-fed antenna arrays using feed networks constructed by slow-wave transmission lines," *IEEE Antennas Wireless Propag. Lett.*, Vol. 15, 798–801, 2016.

10. Loecker, C., C. G. Salzburg, K. Herbertz, and T. Bertuch, "Series feeding network based on metamaterial compensation lines," *IEEE J. Multiscale Multiphys. Comput. Techn.*, Vol. 2, 142–146, 2017.

11. Lai, A., K. M. K. H. Leong, and T. Itoh, "Novel series divider for antenna arrays with arbitrary element spacing based on a composite right/left-handed transmission line," *Proc. 2005 Eur. Microw. Conf. (EuMC)*, 145–148, Paris, France, Oct. 2005.

12. Bemani, M. and S. Nikmehr, "Dual-band N-way series power divider using CRLH-TL metamaterials with application in feeding dual-band linear broadside array antenna with reduced beam deterioration," *IEEE Trans. Circuits Syst. I, Reg. Papers*, Vol. 60, No. 12, 3239–3246, Dec. 2013.

13. Ueda, T., S. Yamamoto, Y. Kado, and T. Itoh, "Pseudo-traveling-wave resonator with magnetically tunable phase gradient of fields and its applications to beam-steering antennas," *IEEE Trans. Microw. Theory Techn.*, Vol. 60, No. 10, 3043–3054, Oct. 2012.

14. Ueda, T., Y. Kubo, T. Kaneda, M. Hara, Y. Takahashi, and T. Itoh, "Dispersion-free and tunable nonreciprocities in composite right-/left-handed metamaterials and their applications to beam squint reduction in leaky-wave antennas," *IEEE Trans. Microw. Theory Techn.*, Vol. 67, No. 6, 2227–2237, Jun. 2019.

15. Eleftheriades, G. V., M. A. Antoniades, and F. Qureshi, "Antenna applications of negative-refractive-index transmission-line structures," *IET Microw. Antennas Propag.*, Vol. 1, No. 1, 12–22, Feb. 2007.

16. Antoniades, M. A. and G. V. Eleftheriades, "A CPS leaky-wave antenna with reduced beam deterioration using NRI-TL metamaterials," *IEEE Trans. Antennas Propag.*, Vol. 56, No. 3, 708–721, Mar. 2008.

17. Kossifos, K. M. and M. A. Antoniades, "A NRI-TL metamaterial leaky-wave antenna radiating at broadside with zero beam-deterioration," *IEEE Antennas Wireless Propag. Lett.*, Vol. 17, No. 12, 2223–2227, Dec. 2018.

18. Li, H., X. Guo, T. Yu, L. Zhu, and W. Wu, "Wideband continuously tunable phase shifter with phase slope tunability and low phase error," *IEEE Trans. Microw. Theory Techn.*, Vol. 70, No. 4, 2147–2155, Apr. 2022.

19. Wi, S.-H., Y.-S. Lee, and J.-G. Yook, "Wideband microstrip patch antenna with U-shaped parasitic elements," *IEEE Trans. Antennas Propag.*, Vol. 55, No. 4, 1196–1199, Apr. 2007.